Soil reinforcement for seismic design of geotechnical structures

Radoslaw L. Michalowski*

Department of Civil Engineering, The Johns Hopkins University, Baltimore, MD 21218, USA

Abstract

The kinematic theorem of limit analysis is used to evaluate the amount of reinforcement necessary to prevent collapse of slopes. The results are also applicable to some failure modes of reinforced walls. Calculations were performed assuming uniform and linearly increasing distributions of reinforcement strength through the slope height. The computational results are presented in charts, which can be used in design. The seismic influence is substituted with a quasi-static horizontal force. While such an approach ignores the acceleration history and does not allow any insight into the behavior of a structure, it is being routinely used in practice, and the charts are offered as a design aid to determine the amount or strength of reinforcement. The length of reinforcement was also calculated, based on collapse mechanisms which include rupture in some layers and pull-out in others. It was found that the distribution of reinforcement with variable spacing, to match the triangular distribution of "smeared" strength, is more economical than a uniform spacing. Uniform spacing requires longer reinforcement and larger strength. © 1998 Elsevier Science Ltd. All rights reserved.

1. Introduction

Reinforcement of soil structures such as slopes and walls has become an accepted engineering practice in the last 20 years. Reports on the behavior of reinforced soil structures during seismic events emphasize a relatively small distress caused by shaking (see e.g. [1]). White and Holtz [2] noticed that during the Northridge earthquake "No adverse performance of geosynthetic-reinforced structures was observed, even in areas where other types of structures experienced failures and/or other poor performance." It is then natural to seek some guidelines as to how much reinforcement is necessary to adequately protect structures from possible damage due to

* Fax: + 1-410-516-7473; e-mail: rlm@jhu.edu

earthquakes. The most common method used for reinforced soil structures is the quasi-static analysis where the seismic influence is substituted with a static force, usually in the horizontal direction. This method has been used in design of massive retaining walls for more than 50 years, and was adapted for reinforced soil in the 1980s [3]. A ''sliding block analysis'' can be performed to approximately evaluate the displacements of the structure during a seismic event. While used to determine displacement of slopes since the 1960s, it was adapted to reinforced soil structures only recently (see e.g. [4,5]). Numerical calculations, such as the finite element method, did not gain popularity for reinforced soil analysis due to complexities with modeling of the soil-reinforcement interface. A comprehensive review of the techniques used for seismic analysis of geosynthetic-reinforced walls, slopes and embankments was presented recently by Bathurst and Alfaro [6].

Substitution of a quasi-static force for the dynamic effect due to seismic shaking is a rather approximate method. It does not give any insight into the behavior of a structure, it neglects the seismic process (acceleration history), cannot yield any information about permanent displacements of the structure, yet it seems to be a widely accepted design technique. It is useful then to produce charts to aid such design. While attempts have been made in the past at quasi-static analysis of reinforced soil structures [3], more comprehensive calculations to include complex collapse modes including both the rupture (or plastic tensile failure) and pullout of reinforcement, and direct sliding, have been presented only recently [5]. A similar task is undertaken in this paper, although the technique used is different, and calculations are made for both uniform and variable spacing of reinforcement, corresponding to uniform and triangular distributions of ''smeared'' reinforcement strength. Calculations of stability for complex failure modes including simultaneous plastic flow (or rupture) of some reinforcement layers and pull-out of others also differ from those in [5]. The technique used here was applied earlier only to uniformly reinforced slopes with no seismic influence [7]. The respective terms including the quasi-static horizontal forces are now included.

2. Limit analysis of reinforced soil

The kinematic approach of limit analysis, with a quasi-static seismic force in the horizontal direction, is used here to arrive at reinforcement strength and length, and the results are presented in the form of design charts. Limit analysis has been applied to reinforced soil in the last 10 years or so. Two approaches can be distinguished in limit analysis of reinforced soil: (a) the continuum approach, where the soil and reinforcement are first homogenized, and the limit analysis is then applied to the anisotropic continuum, and (b) the structural approach, in which the soil and reinforcement are considered as two separate structural components. The latter is also referred to as a ''mixed'' approach [8], since the reinforcement constitutes structural members, and the soil is considered as a continuum. Examples of the application of limit analysis in reinforced soil can be found in papers by de Buhan et al. [9], Sawicki and Leśniewska [10], de Buhan and Salenşon [11], and others [7,8,12].

It is assumed in the kinematic approach of limit analysis that the soil and rein-forcement are perfectly plastic and their deformation is governed by the associative flow rule

$$\dot{\varepsilon}_{ij}^{pl} = \dot{\lambda}\frac{\partial f(\sigma_{ij})}{\partial \sigma_{ij}}, \quad \begin{array}{l} \dot{\lambda} \geqslant 0 \;\; \text{if } f = 0 \\ \dot{\lambda} = 0 \;\text{if } f < 0 \end{array} \tag{1}$$

where $\dot{\lambda}$ is a nonnegative scalar multiplier, and $f(\sigma_{ij}) = 0$ is the yield criterion. We will assume here that the Mohr–Coulomb failure criterion holds for soils. The con-sequence of the normality rule in Eq. (1) is a well-defined dilatancy rate during plastic deformation. If velocity discontinuities (rupture surfaces) appear in the fail-ure mechanism, the discontinuity vectors ("velocity jumps") must be inclined to the discontinuities at angle of internal friction φ.

The technique of calculations is based on the kinematic theorem of limit analysis. This theorem states that *the rate of work done by traction and body forces is less than or equal to the rate of energy dissipation in any kinematically admissible failure mechanism*

$$\int_V \sigma_{ij}^* \dot{\varepsilon}_{ij}^* \mathrm{d}V \geqslant \int_S T_i v_i \mathrm{d}S + \int_V X_i v_i^* \mathrm{d}V, \quad i,j = 1,2,3 \tag{2}$$

where $\dot{\varepsilon}_{ij}^*$ is the strain rate in a kinematically admissible velocity field, σ_{ij}^* is the stress tensor associated with $\dot{\varepsilon}_{ij}^*$, velocity $v_i^* = v_i$ on boundary S (given kinematic boundary condition), X_i is the vector of body forces (unit weight and the distributed quasi-static inertial force), and S and V are the loaded boundary and the volume, respec-tively. A more comprehensive description of this method can be found in [13,14].

No pore water pressure or liquefaction potential is considered here. This paper deals primarily with slopes, but the results also can be used in analysis of some fail-ure modes of reinforced walls. The slopes considered here are not loaded on their boundaries, so that the first integral on the right-hand side of Eq. (2) is zero. The stability problem is formulated for a given slope with an unknown amount of rein-forcement necessary to prevent failure. Thus, the inequality in Eq. (2) will provide the lower bound to the strength (or amount) of reinforcement.

An alternative technique to solving the limit state problem is the traditional "limit equilibrium" method. One can prove that, provided the same admissible collapse mechanisms are used in the kinematic limit analysis and in the limit equilibrium method, the results must be identical. The kinematic method is utilized herein, since the kinematics of collapse mechanisms appeals to engineering intuition better than the distribution of forces. The limit equilibrium method was applied to reinforced slopes in [15,16].

3. Distribution of reinforcement

Most design suggestions available today assume the linear (increasing with depth) distribution of the reinforcement force. In limit state design this reinforcement force

must be interpreted as the limit force, otherwise the mechanism of collapse considered in the limit analysis (or limit equilibrium method) is not admissible. Thus, if reinforcement layers of equal strength are used, the triangular distribution of the reinforcement force implies reinforcement distribution of the type in Fig. 1(a). From geometrical considerations one can calculate depth z_i of each layer of reinforcement ($i = 1,2,3...n$) assuming that every layer is placed at the centroid of its respective trapezoidal distribution segment:

$$z_i = \frac{2}{3}nH\left[\sqrt{\left(\frac{i}{n}\right)^3} - \sqrt{\left(\frac{i-1}{n}\right)^3}\right], \quad i = 1, 2...n \tag{3}$$

where n is the number of layers. For a uniformly reinforced structure [Fig. 1(b)] the depth of layers can be calculated as

$$z_i = (i - 0.5)\frac{H}{n}, \quad i = 1, 2...n \tag{4}$$

The average strength of the reinforcement in the structure can be represented as

$$k_t = \frac{nT_t}{H} \tag{5}$$

or, in a dimensionless form

$$\frac{k_t}{\gamma H} = \frac{nT_t}{\gamma H^2} \tag{6}$$

where T_t is the tensile strength of a single reinforcement layer (per unit width), n is the number of reinforcement layers, H is the slope height, and γ is the unit weight of the soil. It is then k_t and the length of the reinforcement which need to be determined from the analysis.
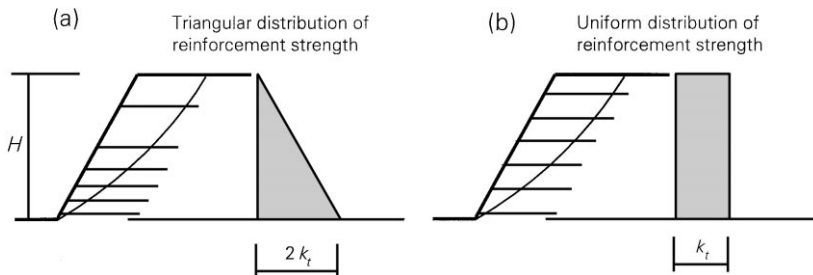

Fig. 1. Schematic of reinforcement in slopes: (a) variable spacing, and (b) uniform spacing.

4. Collapse mechanism and seismic considerations

This paper focuses on reinforced slopes; in particular, the amount of reinforcement and its length necessary to avoid collapse during seismic events is sought. The results also will be applicable to walls, although design of walls requires consideration of additional failure modes not presented here.

It was found earlier [7,15,16] that the rotational log-spiral failure mechanism, as presented in Fig. 2(a), is the most adverse collapse mode, i.e. preventing it requires more reinforcement than preventing other, for instance, translational failure modes. Such a mechanism for slopes without reinforcement was considered earlier by Chen et al. [17]. For a given slope inclination and internal friction angle of the soil, the toe log-spiral failure surface is fully described by two parameters: θ_0 and θ_h [see Fig. 2(a)].

Rupture of the reinforcement is interpreted here as a plastic flow process consistent with the flow rule in Eq. (1). The energy dissipation rate in a single layer of reinforcement intersecting a velocity discontinuity can be derived assuming that the discontinuity is a finite-thickness layer with a high velocity gradient [Fig. 3(a)]. The reinforcement considered here is of a geosynthetics type (geogrids or geotextile), and it contributes to the stability of the structure only through its tensile strength (this reinforcement's resistance to shear, torsion and bending is negligible). Kinematical admissibility requires that the velocity jump vector, [v], be inclined to the velocity discontinuity at angle of internal friction φ. If the reinforcement is inclined to the velocity discontinuity at angle η [Fig. 3(a)], then, assuming no reinforcement pull-out occurs, sector AB of length $t/\sin\eta$ (t being the thickness of the layer) is subjected to plastic flow. Thus, the work dissipation rate in a single layer of reinforcement intersecting a velocity discontinuity (per unit width of the reinforcement) can be calculated as
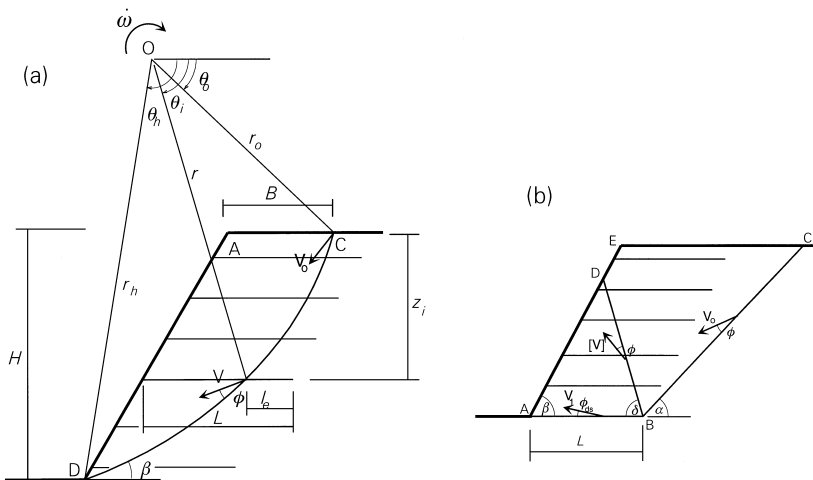

Fig. 2. Collapse mechanisms of slopes: (a) rotational mode, and (b) direct sliding over a single reinforcement layer.

Fig. 3. Plastic flow of reinforcement at a velocity discontinuity: (a) a single reinforcement layer intersecting velocity discontinuity, and (b) schematic for calculations of work dissipation rate along a log-spiral discontinuity.

$$\dot{D} = \int_{0}^{t/\sin\eta} T_t\langle\dot{\varepsilon}_l\rangle\mathrm{d}x = T_t[v]\cos(\eta - \varphi) \tag{7}$$

where T_t is the limit tensile force in the reinforcement sheet per unit width (taken as positive), and the strain rate in the reinforcement is taken as positive in tension $\langle\dot{\varepsilon}_l\rangle = [v]\cos(\eta - \varphi)/t\sin\eta$, and $\langle\dot{\varepsilon}_l\rangle = 0$ when $\eta - \varphi > \pi/2$ (the ability of reinforcement to resist compression is disregarded due to possible buckling and kinking). If the reinforcement is represented in terms of its average strength k_t, as in Eq. (5), the dissipation rate per unit area of the discontinuity surface becomes

$$\dot{D} \int_{0}^{t/\sin\eta} k_t\langle\dot{\varepsilon}_l\rangle\sin\eta\mathrm{d}x = k_t[v]\cos(\eta - \varphi)\sin\eta \tag{8}$$

For a log-spiral failure surface, the energy dissipation rate per infinitesimal length increment, Fig. 3(b), is

$$\mathrm{d}\dot{D} = k_t r\mathrm{d}\theta\frac{\cos(\theta - \varphi)}{\cos\varphi}\mathbf{n}\cdot\mathbf{v} \tag{9}$$

where $\mathbf{v}$ is the velocity discontinuity vector along the log-spiral [Fig. 2(a)], and $\mathbf{n}$ is a unit vector in the direction of reinforcement. The radius of the log-spiral is $r = r_0\exp\{(\theta - \theta_0)\tan\varphi\}$ and the magnitude of the velocity jump vector along the log-spiral is $v = v_0\exp\{(\theta - \theta_0)\tan\varphi\} = \dot{\omega}r_0\exp\{(\theta - \theta_0)\tan\varphi\}$, hence

$$\mathrm{d}\dot{D} = k_t\dot{\omega}r_0^2(\sin\theta\cos\theta + \sin^2\theta\tan\varphi)e^{2(\theta-\theta_0)\tan\varphi}\mathrm{d}\theta \tag{10}$$

and, integrating from θ_0 to θ_h and assuming that $k_t = $ const. [Fig. 1(b)], we have

$$\dot{D} = \frac{1}{2}k_t\dot{\omega}r_0^2(\sin^2\theta_h e^{2(\theta_h-\theta_0)\tan\varphi} - \sin^2\theta_0) \tag{11}$$

where $\dot{\omega}$ is the velocity of rotation about point O. Similarly, for the triangular distribution of reinforcement strength [Fig. 1(a)] we obtain

$$\dot{D} = \frac{1}{3} k_t \dot{\omega} r_0^2 (2 \sin^2 \theta_h e^{2(\theta_h - \theta_0)\tan\varphi} - \sin\theta_0 \sin\theta_h e^{(\theta_h - \theta_0)\tan\varphi} - \sin^2\theta_0) \tag{12}$$

The rate of work of the soil weight and the quasi-static inertial force can be calculated as the work rate of block CDOC minus the work rates for blocks ACOA and ADOA [Fig. 2(a)]. Only the horizontal quasi-static force is considered here. Consequently, this work rate takes the form

$$\dot{W} = \gamma r_0^3 \dot{\omega}[f_1 - f_2 - f_3 + k_h(f_1^s - f_2^s - f_3^s)] \tag{13}$$

where seismic coefficient k_h represents the intensity of the distributed horizontal inertial force as a fraction of the soil unit weight, γ. Coefficients f_1, f_2, f_3, and f_1^s, f_2^s, and f_3^s are functions of the slope inclination angle (β), the geometry of the failure surface (θ_0, θ_h), and the internal friction angle of the soil (φ). The first three functions were derived earlier by Chen et al. [17], and they all are given in the Appendix.

Substituting now the expressions for the rate of energy dissipation [Eqs. (11) or (12)] for the left-hand side of Eq. (2) and the rate of work of the weight and seismic force for the right-hand side, one obtains the following expressions for the lower bound to the amount of reinforcement necessary to prevent the slope failure

$$\frac{k_t}{\gamma H} = \frac{2[f_1 - f_2 - f_3 + k_h(f_1^s - f_2^s - f_3^s)]}{\sin^2\theta_h e^{2(\theta_h - \theta_0)\tan\varphi} - \sin^2\theta_0} \frac{r_0}{H} \tag{14}$$

for the uniform distribution of reinforcement, and

$$\frac{k_t}{\gamma H} = \frac{3(f_1 - f_2 - f_3 + k_h(f_1^s - f_2^s - f_3^s)]}{2\sin^2\theta_h e^{2(\theta_h - \theta_0)\tan\varphi} - \sin\theta_0 \sin\theta_h e^{(\theta_h - \theta_o)\tan\varphi} - \sin^2\theta_0} \frac{r_0}{H} \tag{15}$$

for the triangular distribution, and r_0/H is found from the geometrical relations in Fig. 2(a)

$$\frac{H}{r_0} = \sin\theta_h e^{(\theta_h - \theta_0)\tan\varphi} - \sin\theta_0 \tag{16}$$

5. Required reinforcement strength

The expressions in Eqs. (14) and (15) now can be used to arrive at the lower bounds to the reinforcement strength for slopes with different inclinations, for a variety of internal friction angles of the soil, and for different intensities of the

seismic force, k_h. An optimization scheme needs to be used in order to find the best lower bound to the required reinforcement. The maximum of $k_t/\gamma H$ was sought from Eqs. (14) and (15), with angles θ_0 and θ_h being variable. A gradiental method of optimization was used, and the results are presented in the design charts in Figs. 4 and 5.

The charts in Fig. 4 present dimensionless average strength $k_t/\gamma H$ of the reinforcement necessary to prevent failure of uniformly reinforced slopes. The charts are given for different intensities of seismic coefficient k_h. The required strength increases with the decrease in the internal friction angle and with the increase in the seismic coefficient k_h and the slope inclination angle β.
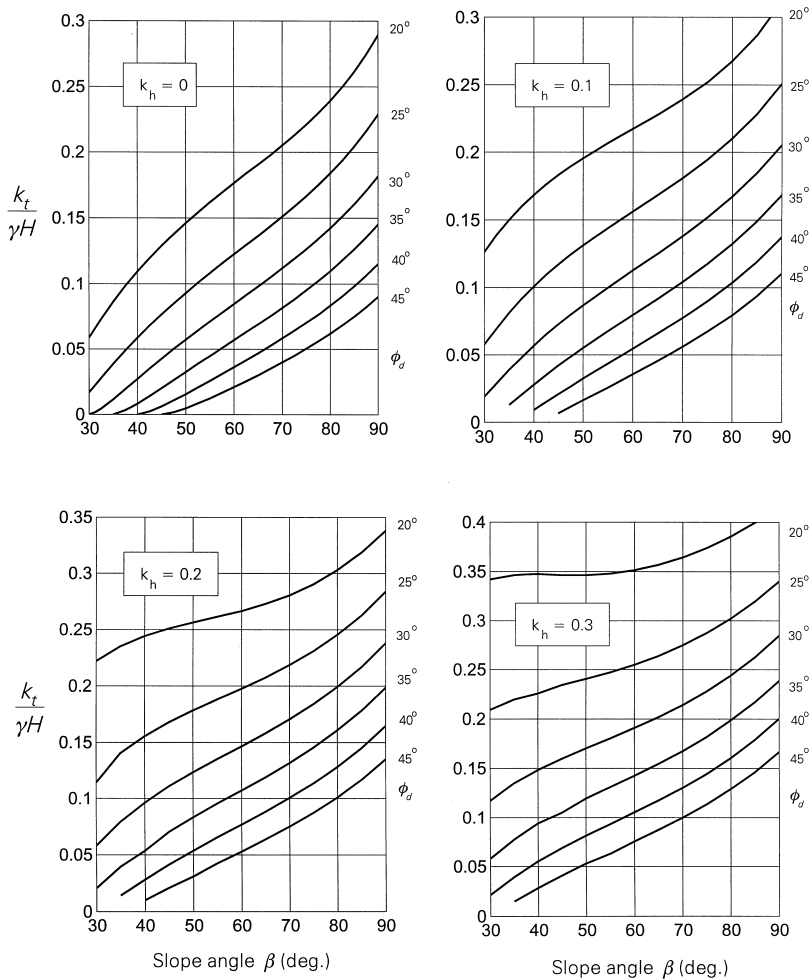
Fig. 4. Reinforcement strength (dimensionless) necessary to prevent slope collapse associated with reinforcement rupture; uniform spacing.
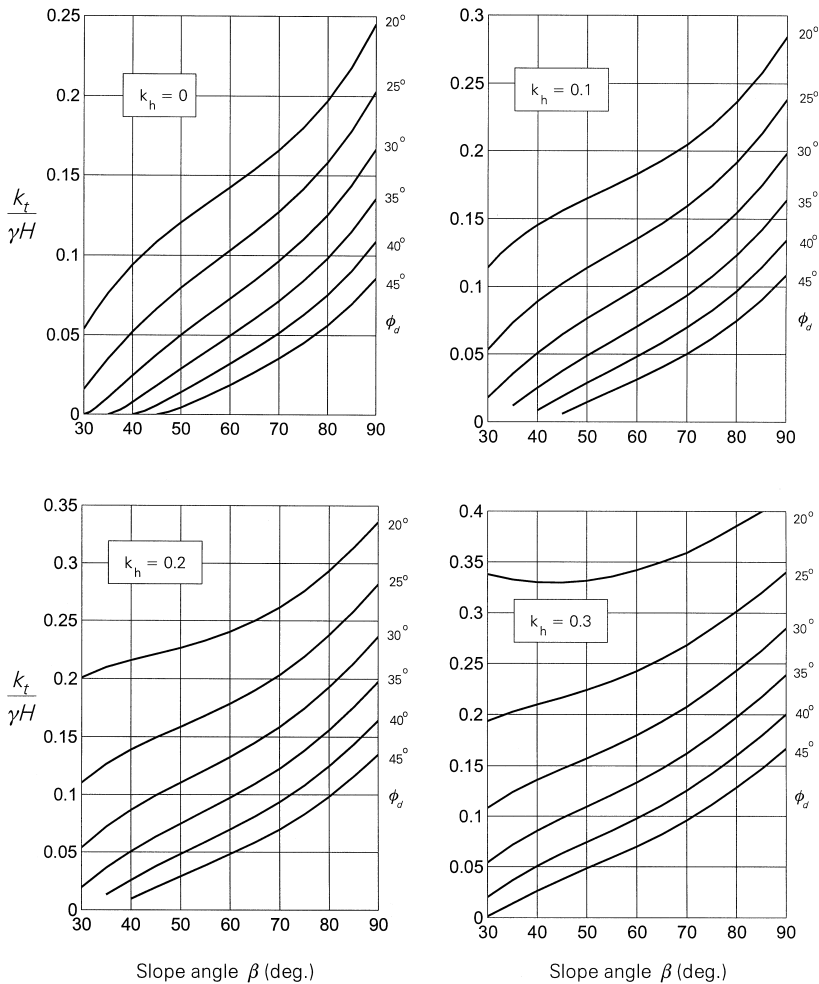
Fig. 5. Reinforcement strength (dimensionless) necessary to prevent slope collapse associated with reinforcement rupture; variable spacing.

Uniformly distributed reinforcement is commonly used for slopes of up to 6 m high. For tall slopes it is more economical to design varied spacing of reinforcement (or step-wise varied spacing). The calculations of the best estimate of the average reinforcement strength were then made assuming a triangular distribution, according to Fig. 1(a) [and Eq. (15)]. The respective charts are shown in Fig. 5. These results appear to be similar to those presented recently by Ling et al. [5] for slopes with selected inclination angles. It follows from Figs. 4 and 5 that the same slope requires more reinforcement if it is uniformly distributed. It may be concluded then that variable spacing leads to a more economic use of geosynthetic material. It was interesting to notice that for very steep structures (typical of walls—nearly 90°) and

large k_h, a translational mechanism ($\theta_0 = \theta_h$) gives the best estimate of $k_t/\gamma H$. For a translational mechanism, however, the energy dissipation rate in the reinforcement during failure is independent of its distribution. Therefore, the results are identical for these cases, whether the reinforcement distribution is uniform or triangular (see, for instance, results for $\beta = 90°$ and $k_h = 0.3$).

The charts in Figs. 4 and 5 now can be utilized to find the necessary amount (or strength) of reinforcement for a given slope (given k_h, and known slope inclination angle β, internal friction angle φ, and unit weight γ). First $k_t/\gamma H$ needs to be read from an appropriate chart, and, upon substitution of k_t into Eq. (5), one can calculate the number of layers if the tensile strength of geosynthetic, T_t, is given, or, for a given number of layers n, one can calculate the necessary strength of a single layer. The depth of the layers can then be calculated either from Eqs. (3) or (4). For practical purposes, the angle of internal friction used in the chart should be reduced according to an appropriate safety factor $F[\varphi_d = \tan^{-1}(\tan\varphi/F)]$.

6. Required length of reinforcement

It has been assumed, so far, that the reinforcement fails by plastic flow referred to here as tensile rupture. This happens only when the reinforcement is of sufficient length, otherwise some reinforcement layers may be pulled out from the soil. The method used here for calculating the required length of reinforcement was proposed earlier [7], with the exception that seismic forces are now considered. The pullout force for a single layer of reinforcement is

$$T_p = 2\gamma z^* l_e f_b \tan\varphi \tag{17}$$

where z^* is the overburden depth and l_e is the effective length [Fig. 2(a)]. The soil-reinforcement friction coefficient is expressed here as a fraction of the tangent of the internal friction angle $f_b \tan\varphi$. The energy dissipation rate during rotational failure needs to be calculated now as a sum of dissipation in all layers that are being pulled out, and in the layers that rupture

$$\dot{D}_p = \sum_{i=1}^{k} T_p r_0 \dot{\omega}\left(\sin\theta_0 + \frac{z_i}{r_0}\right)$$
$$\dot{D}_t = \sum_{i=k+1}^{n} T_t r_0 \dot{\omega}\left(\sin\theta_0 + \frac{z_i}{r_0}\right) \tag{18}$$

where k is the number of layers being pulled out [see Fig. 2(a) for z_i and r_0]. Equating the dissipation rate in Eq. (18) to the work of the body forces in Eq. (13), and noting that $T_t = k_t H/n$, one obtains

$$\frac{k_t}{\gamma H} = \frac{\left(\frac{r_0}{H}\right)^2 [f_1 - f_2 - f_3 + k_h(f_1^s - f_2^s - f_3^s)] - \sum_{i=1}^{k} \frac{T_p}{\gamma H^2}\left(\sin\theta_0 + \frac{z_i}{r_0}\right)}{\frac{1}{n}\sum_{i=k+1}^{n}\left(\sin\theta_0 + \frac{z_i}{r_0}\right)} \tag{19}$$

The length of reinforcement is implicitly included in the pullout force T_p. An economically designed reinforcement length is one that yields $k_t/\gamma H$ in Eq. (19) equal to that in Eq. (14) [or Eq. (15)]. This is explained in Fig. 6. The dimensionless average strength in Fig. 6(a) is calculated from Eqs. (14) or (19), and it corresponds to failure surfaces which intersect the slope surface at a respective ordinate x; for instance, the magnitude of $k_t/\gamma H$ at point A [Fig. 6(a)] corresponds to the failure surface A [Fig. 6(b)]. Out of all failure surfaces, A and B are the two most critical ones (collapse along other surfaces requires lower reinforcement strength). The maximum of $k_t/\gamma H$ at point A relates to the best lower bound with rupture in all layers, [Eq. (14)]. The maximum at B corresponds to the case where the top layer is bypassed by the failure surface and the second layer is pulled out. If the maximum at B was less than that at A, it would be indicative of having the reinforcement longer than necessary. In such a case the all-rupture mechanism would control the collapse.

　　The results of calculations of the reinforcement length are presented in Figs. 7 and 8, for the uniform and variable spacing of reinforcement to match the distributions in Fig. 1(b) and (a), respectively. The soil-reinforcement coefficient of friction was assumed to be $0.8\tan\varphi(f_b = 0.8)$, and 24 layers ($n = 24$) were taken in all calculations. The calculated lengths are designated as $(L/H)_{ovrl}$, since the type of collapse
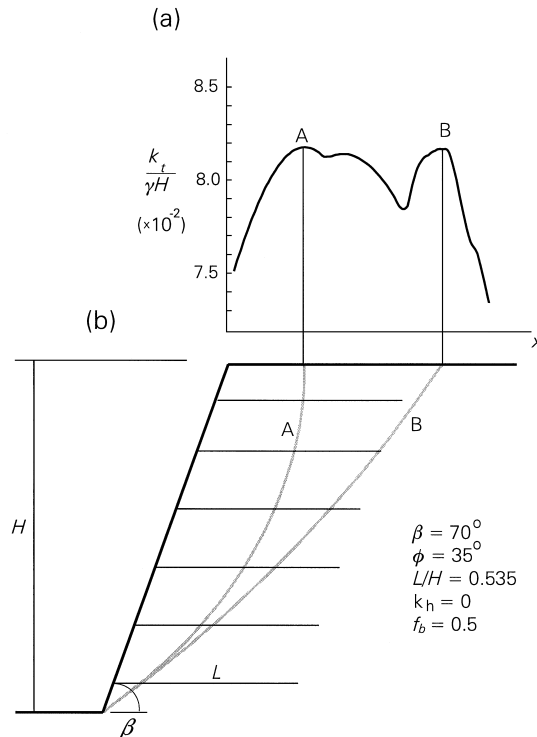

Fig. 6. Criterion for calculating reinforcement length: (a) required strength to prevent failure, and (b) failure surfaces associated with two most adverse failure mechanisms.
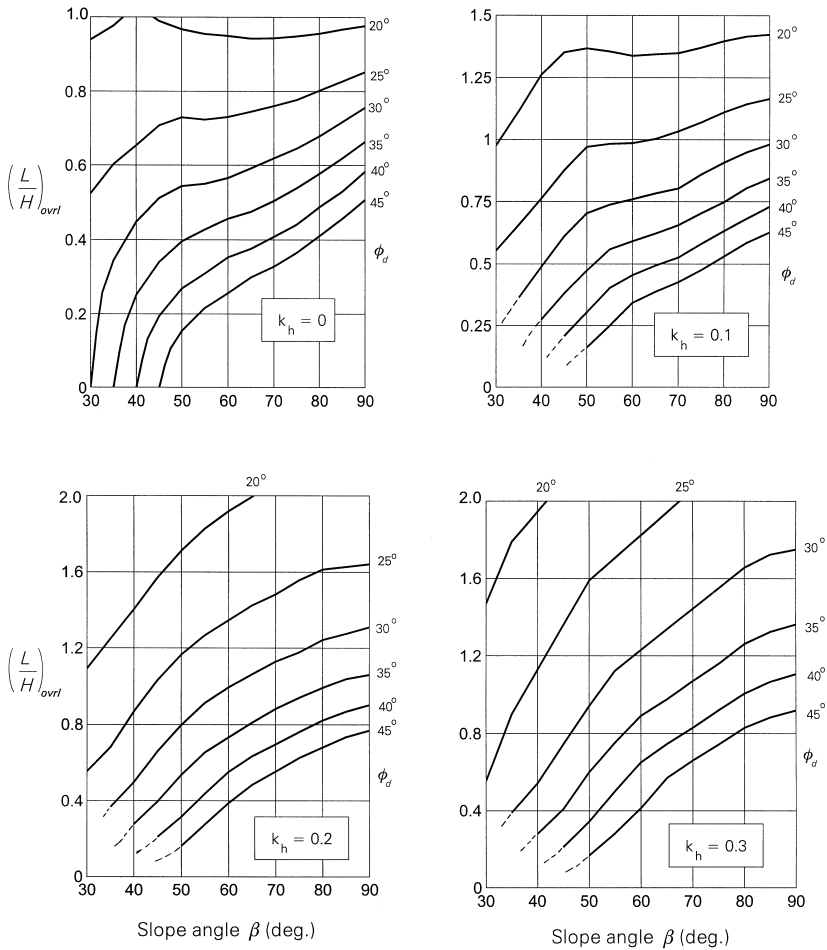
Fig. 7. Reinforcement length required for uniformly reinforced slopes.

considered is often referred to as an overall failure. These are the best lower bounds to the reinforcement length necessary to prevent failure. The maximum of L/H was calculated from Eq. (19) (L is implicitly included in T_p) with $k_t/\gamma H$ determined from Eq. (14) for the uniform distribution [and with $k_t/\gamma H$ determined from Eq. (15) for the triangular distribution of reinforcement]. The results were obtained numerically, with an optimization scheme in which geometric parameters describing the failure mechanism were taken as variables.

The results clearly indicate that the triangular distribution of reinforcement is more economic: the uniform distribution requires longer reinforcement to prevent failure.

From the limit analysis standpoint the lengths calculated are not rigorous bounds, since the stress on the reinforcement layers was approximately assumed to be equal
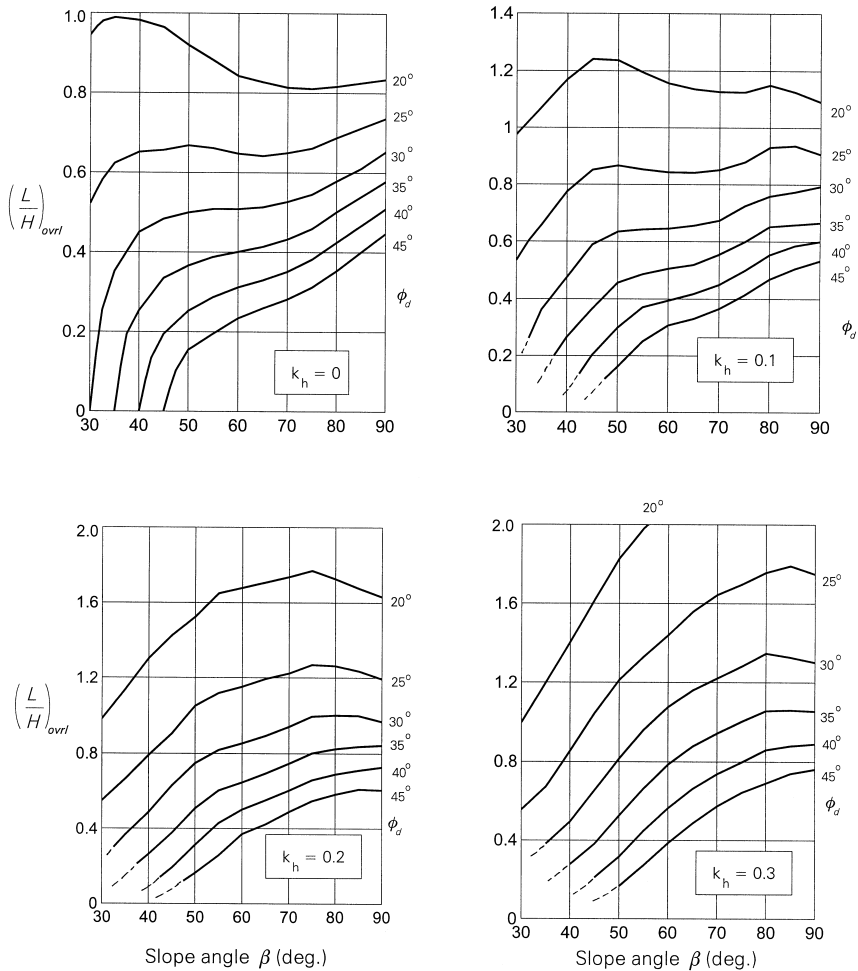
Fig. 8. Reinforcement length required for slopes with triangular distribution of reinforcement strength.

to the overburden pressure. This assumption, however, is commonly used in calculations of pullout forces [15,16].

The last set of calculations was performed assuming a different mode of failure: direct sliding. Direct sliding of the soil mass over the bottom layer of reinforcement is compatible with a translational mechanism in Fig. 2(b). Calculations of a similar type were made recently by Ling et al. [5] in the context of seismic design, although the calculations presented here differ considerably from those in [5] in the way the influence of the reinforcement within the sliding blocks is taken into account. The geosynthetic-soil coefficient of friction for both the direct sliding and pullout was assumed to be equal to $0.8 \tan \varphi (f_d = f_b = 0.8)$, and 24 layers of reinforcement were assumed. Angles α and δ were taken as variables in an optimization procedure where

the maximum of length L [Fig. 2(b)] was sought. Rupture of reinforcement or the pullout force, whichever smaller, was considered along failure surface BD. A more detailed description of a similar mechanism can be found elsewhere [7].

The length of reinforcement necessary to prevent direct sliding is shown in Fig. 9. The difference in calculated length for uniform and variable spacing of reinforcement appeared to be rather small (a few per cent), therefore only one set of results is presented (uniform spacing). The reinforcement length increases significantly with the increase in seismic coefficient k_h. The lengths calculated are not as large as those published recently by Ling et al. [5]. This is because here the effect of the reinforcement between the sliding blocks is accounted for.
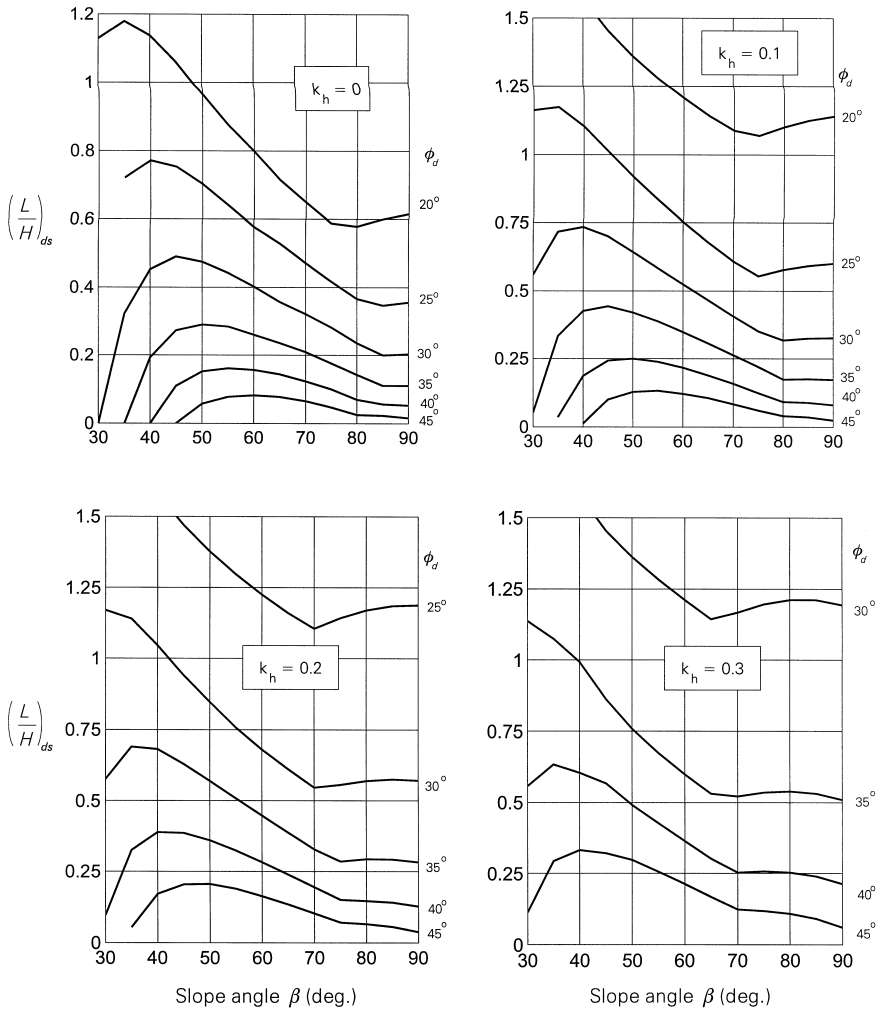

Fig. 9. Reinforcement length required to prevent direct sliding.

7. Final remarks

Seismic design considerations, where dynamic forces are substituted with quasi-static ones, are very approximate in nature, and they do not give any insight into the behavior of structures. It is an accepted practice, however, to include quasi-static forces as a means of seismic design. The charts produced can then be used as a design aid. These charts are presented for both the uniform and triangular distribution of the reinforcement strength.

Slopes up to about 6 m tall are routinely designed with evenly spaced reinforcement. While this may be feasible economically, the reinforcement is better used if its spacing is varied to approximately match the triangular distribution of the strength. Uniform spacing requires longer reinforcement and larger strength.

The reinforcement length obtained from the calculations increases significantly with an increase in the quasi-static force, and, for large seismic accelerations, the design according to the quasi-static method may not be feasible. This has been already raised in the literature [5]. It may be more appropriate to allow the structure be subjected to larger-than-critical accelerations, and to introduce a displacement design criterion. Given the history of ground acceleration in a seismic event, the expected displacement can be calculated by twice integrating its acceleration beyond the critical acceleration of the structure. Such a method has been used for geotechnical structures for many years [18], and it was suggested recently that it be applied to reinforced soil structures [4,5]. While such an analysis was not in the scope of this paper, it should be considered when the reinforcement length from the quasi-static analysis exceeds a reasonable length (e.g. 1.5H).

Acknowledgements

Appendix A

Functions f_i and $f_l^s (i = 1, 2, 3)$ used Eq. (13) for the description of the rate of work of the soil weight and quasi-static inertial forces are given below. These functions were derived based on geometrical relations in Fig. 2(a) (the first three were previously given in [17]):

$$f_1 \frac{1}{3(1 + 9\tan^2 \varphi)}[(3\tan\varphi \cos\theta_h + \sin\theta_h)e^{3(\theta_h - \theta_0)\tan\varphi} - 3\tan\varphi \cos\theta_0 - \sin\theta_0] \qquad (A1)$$

$$f_2 = \frac{1}{6}\frac{B}{r_0}\left(2\cos\theta_0 - \frac{B}{r_0}\right)\sin\theta_0 \qquad (A2)$$

$$f_3 = \frac{1}{6}\frac{H}{r_0}\frac{\sin(\beta + \theta_h)}{\sin\beta}\left(2\cos\theta_h e^{(\theta_h - \theta_0)\tan\varphi} + \frac{H}{r_0}\cot\beta\right)e^{(\theta_h - \theta_0)\tan\varphi} \tag{A3}$$

$$f_1^s = \frac{1}{3(1 + 9\tan^2\varphi)}[(3\tan\varphi\sin\theta_h - \cos\theta_h)e^{3(\theta_h - \theta_0)\tan\varphi} - 3\tan\varphi\sin\theta_0 + \cos\theta_0] \tag{A4}$$

$$f_2^s = \frac{1}{3}\frac{B}{r_0}\sin^2\theta_0 \tag{A5}$$

$$f_3^s = \frac{1}{6}\frac{\sin(\beta + \theta_h)}{\sin\beta}\left(2\sin\theta_h e^{(\theta_h - \theta_0)\tan\varphi} + \frac{H}{r_0}\right)e^{(\theta_h - \theta_0)\tan\varphi} \tag{A6}$$

where

$$\frac{B}{r_0} = \frac{1}{\sin\theta_h}\left[\sin(\theta_h - \theta_0) - \frac{H}{r_0}\frac{\sin(\beta + \theta_h)}{\sin\beta}\right] \tag{A7}$$

and the ratio H/r_0 is given in Eq. (16).

References

[1] Tatsuoka F, Tateyama M, Koseki J. Performance of geogrid-reinforced soil retaining walls during the Great Hanshin–Awaji earthquake. 1st International Symposium on Earthquake Geotechnical Engineering, Tokyo, 1995. p. 55–60.

[2] White DM, Holtz RD. Performance of geosynthetic-reinforced slopes and walls during the Northridge, California earthquake of 17 January, 1994, Report, University of Washington, Seattle, 1995.

[3] Bonaparte R, Schmertmann GR, Williams ND. Seismic design of slopes reinforced with geogrids and geotextiles. 3rd International Conference on Geotextiles, vol. 1, Vienna, 1986. p. 273–8.

[4] Cai S, Bathurst RJ. Deterministic sliding block methods for estimating seismic displacements of earth structures. Soil Dynamics and Earthquake Engineering 1996;15:255–68.

[5] Ling HI, Leshchinsky D, Perry EB. Seismic design and performance of geosynthetic-reinforced soil structures. Géotechnique 1997;47:933–52.

[6] Bathurst RJ, Alfaro MC. Review of seismic design, analysis and performance of geosynthetic reinforced walls, slopes and embankments. International Symposium on Earth Reinforcement, keynote lecture, Kyushu, 1996. p. 23–52.

[7] Michalowski RL. Stability of uniformly reinforced slopes. J. Geot. Geoenv. Engrg. 1997;123:546–56.

[8] Anthoine A. Mixed modelling of reinforced soils within the framework of the yield design theory. Computers and Geotechnics 1989;7:67–82.

[9] de Buhan P, Mangiavacchi R, Nova R, Pellegrini G, Salenşon J. Yield design of reinforced earth walls by homogenization method. Géotechnique 1989;39:189–201.

[10] Sawicki A, Leśniewska D. Limit analysis of cohesive slopes reinforced with geotextiles. Computers and Geotechnics 1989;7:53–66.

[11] de Buhan P, Salenşon J. A comprehensive stability analysis of soil nailed structures. Eur. J. Mech., A/Solids 1993;12:325–45.

[12] Michalowski RL, Zhao A. Continuum versus structural approach to stability of reinforced soil. J. Geot. Engrg. 1995;121:152–62.

[13] Chen WF. Limit analysis and soil plasticity. Amsterdam: Elsevier, 1975.

[14] Salenşon J. An introduction to the yield design theory and its applications to soil mechanics. Eur. J. Mech., Ser. A/Solids 1990;9:477–500.

[15] Jewell RA, Revised design charts for steep reinforced slopes. In: Reinforced embankments, theory and practice. (ed. DA Shercliff) London: Thomas Telford, 1990:1–30.

[16] Leshchinsky D, Boedecker RH. Geosynthetic reinforced soil structures. J. Geot. Eng. 1989;115:1459–78.

[17] Chen WF, Giger MW, Fang HY. On the limit analysis of stability of slopes. Soils and Foundations 1969;9(4):23–32.

[18] Newmark NM. Effects of earthquakes on dams and embankments. Géotechnique 1965;15:139–160.